



Published in final edited form as:

Lab Chip. 2011 February 7; 11(3): 398–406. doi:10.1039/c0lc00296h.

A surface topography assisted droplet manipulation platform for biomarker detection and pathogen identification†

Yi Zhang^{‡,a}, Seungkyung Park^{‡,b}, Kelvin Liu^a, Jennifer Tsuan^a, Samuel Yang^b, and Tza-Huei Wang^{*,c}

^aDepartment of Biomedical Engineering, Johns Hopkins University, Baltimore, Maryland, U.S.A

^bDepartment of Emergency Medicine, Johns Hopkins University, Baltimore, Maryland, U.S.A

^cDepartment of Biomedical Engineering, Department of Mechanical Engineering, Sidney Kimmel Comprehensive Cancer Centre, Centre of Cancer Nanotechnology Excellence at Johns Hopkins, Johns Hopkins University, Baltimore, Maryland, U.S.A

Abstract

This paper reports a droplet microfluidic, sample-to-answer platform for the detection of disease biomarkers and infectious pathogens using crude biosamples. The platform exploited the dual functionality of silica superparamagnetic particles (SSP) for solid phase extraction of DNA and magnetic actuation. This enabled the integration of sample preparation and genetic analysis within discrete droplets, including the steps of cell lysis, DNA binding, washing, elution, amplification and detection. The microfluidic device was self contained, with all reagents stored in droplets, thereby eliminating the need for fluidic coupling to external reagent reservoirs. The device incorporated unique surface topographic features to assist droplet manipulation. Pairs of micro-elevations were created to form slits that facilitated efficient splitting of SSP from droplets. In addition, a compact sample handling stage, which integrated the magnet manipulator, the droplet microfluidic device and a Peltier thermal cycler, was built for convenient droplet manipulation and real-time detection. The feasibility of the platform was demonstrated by analysing ovarian cancer biomarker Rsf-1 and detecting *Escherichia coli* with real time polymerase chain reaction and real time helicase dependent amplification.

Introduction

Infectious disease is the second most common cause of death according to WHO.¹ Compared with conventional culture based approaches, genetics based molecular diagnostics have greatly reduced the turn-around time for the identification of infectious agents. Another major cause of death is cancer.¹ The concepts of early cancer detection and personalized medicine by analyzing a patient's genetic biomarkers may allow timely initiation of targeted treatment and improve clinical outcomes.^{2,3} With genetic detection

†Electronic supplementary information (ESI) available: Supplementary Fig. S1–S6 and supplementary video, which demonstrates topography assisted droplet manipulation with food dye as a visual aid. See DOI: 10.1039/c0lc00296h

Corresponding: thwang@jhu.edu; Tel: (+001) 4105167086.

[‡]These authors contributed equally.

being more and more popular, low-cost, easily accessible and fully functional DNA detection systems are highly desirable. One major application of micro total analysis systems (μ TAS) is to perform molecular diagnostics at the point-of-care to enable timely clinical decision and treatment.

During past decades, great effort has been put into the development of miniaturized platforms for biological and chemical analyses.⁴⁻¹² The advantages of these microfabricated devices include fast analysis, low sample and reagent consumption, low cost, high portability and disposability. Such miniaturization efforts have led to the development of μ TAS, systems capable of integrated sample preparation, biochemical reaction, and analyte detection through microfluidic manipulations.¹³⁻¹⁵ Conventional continuous flow microfluidic systems have made considerable progress towards integrating multiple tasks onto a single platform. However, most of these platforms are not amenable in point-of-care utilizations, in part because they incorporate complicated microfluidic components such as microvalves, micropumps and interface connections. Moreover, conventional microfluidic bioanalytical platforms often require bulky and expensive peripheral accessories that are not practically portable.

Droplet-based microfluidic devices have recently garnered increasing attention.¹⁶⁻³¹ One major form of droplet microfluidic device manipulates droplets on an open surface. Such droplets are self contained and function both as reaction chambers and fluid transportation units.¹⁹⁻²² Many actuation methods have been developed to control the droplet movement, including passive actuation^{26,27} and active actuation, such as dielectrophoresis,^{17,28} surface acoustic wave,¹⁹ electrowetting^{17,31} or magnetic forces.^{20-23,29} Among all the actuation methods, magnet-actuated droplet manipulation has special advantages because of its flexibility and easy operation. The use of a permanent magnet circumvents the need for external fluidic control units, hence greatly reducing the fabrication and operation cost. Furthermore, this valveless and pumpless droplet platform is extremely useful for point-of-care applications due to its reduced complexity, high portability, and the capability of onchip storage of reagents in droplets. In addition, the magnetic particles used for droplet actuation can also serve as carriers for biomolecules, such as when silica superparamagnetic particles (SSP) are used for nucleic acid binding and transfer. Despite its simplicity, there are factors, such as liquid to particle ratio (L/P ratio) and magnet moving speed, that affect the control of droplets on the surface.³² In many applications, large functional surface area, hence a large number of magnetic particles is required for efficient biomolecule adsorption. However, such conditions may hinder droplet control because the small L/P ratio prevents the splitting of SSP from the droplet.

Although a great number of nucleic acids based assays are currently available, polymerase chain reaction (PCR) remains the dominant technique owing to its simplicity and high sensitivity. Many state-of-the-art biomolecular assays rely heavily on PCR or modified versions of PCR, such as real time PCR,³³ bridging PCR³⁴ and BEAMing PCR.^{24,35} Numerous studies have attempted to translate the PCR assay onto the microfluidic chip and have made great contributions in various aspects, including device fabrication and packaging techniques, materials, microfluidic architecture and handling, and surface modifications.³⁶ Other popular nucleic acid amplification methods mainly fall into the

category of isothermal amplification, in which the reactions are performed at a constant temperature rather than under thermal cycling. Helicase dependent amplification (HDA) mimics the *in vivo* DNA duplication scheme by using helicase to unwind double stranded DNA.^{37–39} Unlike other isothermal amplification approaches, HDA utilizes a much simpler reaction mechanism and exponentially amplifies the target sequence to a detectable level in a reasonably short time period. Although HDA lacks of sensitivity of PCR, the simple thermal management renders it very appealing for point-of-care applications.

One of the preconditions for nucleic acid amplification is to extract the genomic contents from crude biosamples. This sample preparation step removes any inhibitors that may have negative effects on the amplification reactions. Conventional ethanol precipitation based extraction methods require centrifugation and hence are not compatible with the chip format. On the contrary, solid phase extraction, which works by promoting nucleic acid adsorption in a chaotropic environment and desorption in low ionic strength buffers, often employs silica based substrates in the form of either micropillars/microposts^{40,41} or immobilized micro/nano particles.^{21,22,42,43} These materials can be easily incorporated into microfluidic systems. However, the number of separate wash steps and buffers required in these extraction protocols makes operation in typical microfluidic systems both complex and cumbersome.

To address the aforementioned problems and demands, we have developed a droplet microfluidic platform that was able to perform nucleic acids based pathogen identification and biomarker detection from crude biosamples. We utilized SSP to carry out solid phase extraction in discrete droplets. Material transfers were realized by moving, mixing, merging and splitting SSP from the droplets. The SSP provided both the actuation force for droplet movement and the functional substrate for DNA attachment. The microfluidic chips (Fig. 1) incorporated surface topographic features to facilitate the droplet manipulation. The micro surface elevations formed slits to provide high surface tension and friction barriers, allowing SSP to split easily from the droplet.^{44,45} The micro reaction basins held the droplet in position during the amplification reaction, avoiding temperature gradient induced droplet motion. In addition, a sample handling stage (Fig. 2) was designed to integrate the microfluidic chip, the magnet holder and the thermal cycling unit onto a single platform. We validated our platform by successfully detecting Rsf-1 cancer biomarker from whole blood and identifying *Escherichia coli* (*E. coli*) from crude biosamples using real time PCR and HDA.

Methods and materials

Microfluidic chip fabrication

The surface features were made by casting polydimethylsiloxane (PDMS) against a microfabricated mold. For the reverse V-shape micro-elevations (Fig. 1a), a layer of 600 μm of SU-8 photoresist was spun on the silicon substrate by multiple spin coatings, and the patterns were lithographically defined (ESI[†] Fig. S1). The SU-8 mold was hard baked and

[†]Electronic supplementary information (ESI) available: Supplementary Fig. S1–S6 and supplementary video, which demonstrates topography assisted droplet manipulation with food dye as a visual aid. See DOI: 10.1039/c0lc00296h

dip-coated with 1% Teflon AF (Dupont Corp.) before PDMS casting. The PDMS was spun on the mold at 100 rpm for 30 s, resulting in a thin PDMS membrane. Micro reaction basins were created in membrane using a circular punch of 4 mm in diameter. Lastly, the membrane was oxygen plasma treated and rolled onto the glass coverslip using a metal rolling pin. The oxygen plasma bonded device was baked at 80 °C overnight, after which it was dip-coated with 1% Teflon AF and baked at 80 °C for another 24 h. The Teflon coating on the PDMS membrane eased droplet movement across the surface. The mold for creating the micro pillars was designed using the computer aided design (CAD) software SolidWorks (SolidWork Corp.) and created using computer numeric controlled (CNC) machining. We chose polytetrafluoroethylene (PTFE) as the substrate material to reduce surface interactions. The PDMS casting process on the CNC machined mold was the same as the microfabricated mold. Additionally, an optional mini tank was created by bonding a hollow PDMS border around the PDMS membrane to contain the mineral oil. The droplet movement took place either in the air (Fig. 1a) or oil medium (Fig. 1b).

Droplet handling

The handheld sample handling stage (Fig. 2) was designed using SolidWorks and machined from aluminium. The stage comprised a slider, a top sample plate, four mounting poles, a centre cylinder, a magnet bar holder and a base plate. The Peltier heater/cooler was fixed onto a slider that slides beneath the micro reaction basins during nucleic acid amplification. The top sample plate had a cavity in the middle so that the magnets below the plate were able to reach the bottom surface of the chip and manipulate the droplet motion. A vacuum trench was created along the edge of the cavity. Once connected to a vacuum source, it would hold the chip steady. The magnet bar holder was made of the aluminium with a piece of steel fused in the centre region. Hence, the magnets could be easily fixed on the bar. The magnet bar holder was inserted into the slots on the centre cylinder. The magnet bar could be manually controlled with 2 degree of freedom, both along the slots and perpendicular to the slots, hence the droplets could be manoeuvred to any position on the chip. By moving the magnet bar holder along the slots, the magnets actuated the SSP which in turn controlled the motion of the droplets. The sample stage could also operate in automatic mode by replacing the centre cylinder with a 2D translation track.

Thermal control

The temperature control was managed using a miniaturized Peltier heating/cooling system (Ferrotec). Electrical power was supplied by a DC source and an H-bridge amplifier, and regulated by a PID controller using pulse width modulation (PWM) A K-type thermocouple (Omega Engineering) was used to monitor the microfluidic chip temperature. A LabView program, was written to interface the PID controller and record the thermal response of the system.

DNA extraction

Human genomic DNA (gDNA) extraction was performed from the total blood by solid phase extraction (SPE) using SSP. SPE involved the binding of gDNA to the SSP surface in the highionic-strength chaotropic buffer, followed by a few washing steps with organic solvent to remove the salts. Lastly, the gDNA was eluted in low-ionic strength buffers and

collected for subsequent analysis. The pH and temperature were also tuned to control the adsorption and desorption of the gDNA from the SSP surface. Human blood was obtained from healthy individuals after receiving the informed consent and preserved in anticoagulants. Binding buffer, washing buffer and SSP were purchased from Qiagen and prepared according to the manufacturer's protocol. 5 μL of lysis/binding buffer was mixed with 5 μL of isopropanol alcohol (IPA), 0.5 μL of protease and 0.5 μL SSP. The mixture was dispensed onto the chip as a droplet that sat on the surface. One drop of 17.5 μL washing buffer 1 and two drops of 12.5 μL washing buffer 2 were dispensed at their designated locations on the chip (Fig. 1). A 5 μL droplet of nucleic acid amplification reaction mixture, which also functioned as the elution buffer, was dispensed onto the chip. If the chip was operated in air, mineral oil was applied over the reaction buffer droplet in order to prevent evaporation during heating. With all the buffer droplets in position, the device was primed and ready for sample processing.

gDNA extraction from bacteria was performed in a similar fashion. All the buffers were the same, except that 2 μL of lysostaphin and lysozyme were added to the lysis/binding buffer to facilitate the bacteria lysing.

Nucleic acid amplification reaction

All primers were synthesized by the Integrated DNA Technology Inc. The TaqMan probe was synthesized by the Biosearch Inc. All oligonucleotides sequences were listed in Table 1.

Rsf-1 biomarker detection was performed with both real time PCR and HDA. For real time PCR, QuantiTect SYBR Green PCR Kits (Qiagen Corp.) was used. The real time PCR mixture contained 1 \times SYBR Green master mix and primers (forward primer and reverse primer each at 400 nM). The thermal cycling protocol was as follows: 15 min enzyme activation and pre-denaturation at 95 $^{\circ}\text{C}$, 35 cycles of denaturation (95 $^{\circ}\text{C}$ for 30 s), annealing (57 $^{\circ}\text{C}$ for 30 s) and elongation (72 $^{\circ}\text{C}$ for 30 s), followed by a final elongation step for 5 min at 72 $^{\circ}\text{C}$. Real time HDA was performed using the IsoAmp[®] II Universal tHDA Kit (New England Biolab). The real time HDA mixture was prepared according to the manufacturer's instructions except the primer concentration was 100 nM each and EvaGreen was used at 1 \times concentration. The real time HDA was performed by holding at 65 $^{\circ}\text{C}$ for 2.5 h.

E. coli identification was performed using primers and a Taq-Man probe that targeted a region of the 16S rRNA gene. Using the *Taq* PCR core kit (Qiagen Corp), the PCR mixture contained 1 \times Qiagen PCR buffer, 4 dNTPs (each at 200 μM), total of 3 mM Mg^{2+} , 0.05 units μL^{-1} *Taq* polymerase, 200 nM of TaqMan probe and primers each at 800 nM. The thermal cycling protocol was as follows: 5 min pre-denaturation, 40 cycles of denaturation (94 $^{\circ}\text{C}$ for 30 s), annealing (60 $^{\circ}\text{C}$ for 30 s) and elongation (70 $^{\circ}\text{C}$ for 30 s), followed by a final elongation step for 5 min at 70 $^{\circ}\text{C}$.

Real time data acquisition and melting curve analysis

The optical setup configuration is illustrated in Fig. S2 (details in ESI[†]). A light emitting diode (LED) whose spectrum centred at 470 nm was mounted 45 degree to the Peltier

heater/cooler. A 480/BP40 excitation filter and a 520/BP40 emission filter were used to accommodate the fluorophores used in this study, *i.e.* SYBR Green, EvaGreen and FAM. The fluorescence was detected using an avalanche photo diode (APD).

The data acquisition was realized through a LabView programme. For the real time amplification reaction, the fluorescence signal was sampled at 1 Hz with 100 ms bin time.

The melting curve analysis was performed by ramping the temperature at $0.1\text{ }^{\circ}\text{C s}^{-1}$. The fluorescence signal was sampled at 2 Hz with 100 ms bin time. The negative first derivative was taken to determine the melting temperature.

Gel electrophoresis

The purified gDNA was run on a 0.5% agarose gel. The amplicons were run on a 2% agarose gel. In both cases, the gels were run at 8 V cm^{-1} for 90 mins. The gels were then stained with GelStar[®] nucleic acid gel stain (Lonza Group). Gel images were acquired using a Typhoon[™] 9400 variable imager (GE healthcare) with the following settings: 488nm laser excitation, 530SP emission filter, 500V PMT gain and normal sensitivity.

Results and discussion

Device operation

The device (Fig. 1) was first primed with buffer droplets as described in the methods and materials section. To start, 5 μL of sample (human whole blood or *E. coli* culture) was dispensed into the lysis/binding buffer droplet which contained the SSP. The droplet was incubated for 10 min during which the cells were ruptured and the gDNA adsorbed to the SSP surface due to the high ionic strength and the low pH of the lysis/binding buffer. After incubation, the droplet was dragged by the SSP using a permanent magnet below the chip. When the droplet reached the slit, the SSP split from the parent droplet and formed a small plug, which was then moved to the first washing buffer droplet. The major constituents of the washing buffers were organic solvents. The gDNA remained adsorbed to the SSP surface in the washing buffer while the carried-over salts were diluted and washed away. The surface-adsorbed gDNA was washed three times by moving through 3 different washing buffer droplets, which consisted of one drop of washing 1 and two droplets of washing buffer 2, in the same fashion. The gDNA extraction process ended when the SSP plug was separated from the last washing buffer droplet. Thus far, the gDNA remained highly concentrated on the SSP surface and ready for downstream analysis. Droplet manipulation could be performed in air, in which case all droplets sat in air except for the reaction buffer which was covered by a droplet of mineral oil to prevent evaporation during the amplification reaction (Fig. 1a). Alternatively, the process could be carried out in an oil medium by filling the mini tank with the mineral oil. All the droplets were submerged inside the oil (Fig. 1b). In air, the thermal mass is smaller hence allows faster temperature ramping during the amplification reaction. However, when operated in the oil medium, the droplet movement was easier due to the shorter contact line between the droplet and the surface, hence reducing the friction. Furthermore, abundant mineral oil provided a good barrier to prevent direct evaporation. Because the ionic strength and the pH of the reaction buffers favoured the gDNA desorption, our platform was capable of in-line real time target

detection by directly eluting the surface-adsorbed gDNA from the SSP in the PCR or HDA buffer. After the elution, the SSP dragged the reaction buffer droplet into the reaction basin where the PCR or HDA took place. The micro reaction basin prevented the droplets from moving away during the reaction. Moreover, the bottom surface of the micro reaction basin was exposed directly to the glass coverslip without an intermediary layer of PDMS for improved thermal conductivity (video clip available in ESI[†]).

Surface elevation assisted splitting of SSP from droplets

The splitting of SSP from its parent droplet can be characterized by a critical volume, below which the SSP drags the droplet along rather than splits from it. The critical volume generally increases with increasing amounts of SSP.³² On our device, microelevations were designed to form a narrow 500 nm wide slit (Fig. 1). The slit provided a narrow path for the SSP plug while the microelevations stopped the droplet from passing through due to high surface tension and friction. During operation, a permanent magnet was used to pull the SSP plug which dragged the droplet until it reached the slit (Fig. 3). Here the SSP plug split from the parent droplet and passed through the slit while the bulk of the droplet was detained by the microelevations. To aid visualization, we demonstrated droplet manipulation on an open surface with aqueous food dye. Droplet manipulation was conducted in both the air (Fig. 3a) and oil medium (Fig. 3b). The surface topography assisted SSP splitting was performed with ease in a controlled manner. The microelevations enabled the critical volume to become very small ($\sim 1 \mu\text{L}$) and fairly consistent on our device.

To compare the critical volumes on a flat PDMS surface against one with microelevation features, we placed the permanent magnet ~ 5 mm ahead of a droplet containing SSP. Six different quantities of SSP were tested in 4 different liquid types, specifically water, 100% IPA, 70% ethanol and mineral oil (M5904, Sigma-Aldrich). For each specific quantity of SSP, the critical volume of the droplet was determined by increasing the volume of the liquid until which the SSP could no longer drag the droplet but split from it. The measurements were carried out in air. Both the flat PDMS surface and the surface with microelevations were dip-coated with Teflon. As shown in Fig. 4, for all four liquids tested on the flat PDMS surface, the critical volumes become larger with the increasing amount of SSP. In contrast, a small critical volume ($\sim 1 \mu\text{L}$) is observed for the features-containing surface, regardless of the amount of SSP used. These results prove that with the assistance of surface topographic features, the conditions for SSP splitting become independent of droplet size and composition, offering a higher degree of flexibility and ease of manipulation. Whether the SSP plug moves jointly with the droplet or splits from the droplet is governed by the balance between the magnetic force exerted on the SSP, the friction imposed on the droplet along the contact line, and the capillary force that the SSP plug experiences due to the droplet deformation.³² In real world applications, various buffers with different surface tensions are used at different volumes. In addition, many sample preparation processes involve droplet merging, which considerably alters the L/P ratio. If too much SSP is used, it is impossible to split the SSP from the droplet. If too little SSP is used, the magnetic force imposed on the SSP may be insufficient to actuate the droplet. Furthermore, enough SSP must be applied to provide sufficient functional surface area for biomolecule adsorption. Hence, the range of SSP amount which can be used in a multi-procedure process is

extremely narrow, and one must fine tune the SSP amount to accommodate both solid phase extraction and droplet manipulation. In contrast, with the assistance of the surface topographic features, a much wider range of SSP can be used as SSP splitting becomes easier. To that end, a relatively large amount of SSP can be applied for efficient DNA adsorption without complicating magnetic droplet actuation.

Detection of Rsf-1 marker from blood samples

Rsf-1 is a chromatin remodeling gene that is believed to be a promising biomarker for the ovarian cancer diagnosis and prognosis. Ovarian cancer patients with Rsf-1 gene amplification have more severe disease conditions and shorter survival times than those without.⁴⁶

Detection of Rsf-1 was performed using 5 μL of human whole blood sample. The steps of cell lysis, DNA extraction and PCR were performed on the microfluidic droplet chip following the procedure described previously. The experiment was conducted in an oil medium (Fig. 1b). In order to validate the gDNA extraction, we performed a separate experiment in which the gDNA eluted in the reaction buffer droplet was collected and run on a 0.8% agarose gel at 8 V cm^{-1} for 90 min. The isolated gDNA appeared as a gel band $>23 \text{ kbp}$ (Fig. 5), which is the typical size obtained using SPE due to the shearing induced by the mechanical and chemical stress.^{47,48}

The detection was first carried out with real time PCR using SYBR Green dyes. The fluorescence signal from the PCR droplet was continuously monitored by a custom optical detection readout (ESI[†] Fig. S2). Fig. 6 illustrates the representative fluorescence and the temperature profiles during thermal cycling. The heating and cooling rates were estimated to be 1.5°C s^{-1} and 2.8°C s^{-1} respectively which were comparable to commercial thermal cyclers. Signals acquired during the elongation step at each cycle were averaged and plotted against the thermal cycle number to create the real time amplification curve. An inverse relation between the fluorescence and the temperature was observed by overlaying the two profiles (Fig. 6 inset). Successful detection of Rsf-1 gene from the blood sample was demonstrated by the sigmoidal profile of the amplification curve (Fig. 7a). Melting curve analysis was performed to evaluate the amplification specificity. A single peak observed in the negative first derivative graph confirmed the presence of a single species of amplicon (Fig. 7b). The PCR product was further verified by agarose gel electrophoresis (ESI[†] Fig. S3).

Rsf-1 detection was also carried out using real time HDA. The isothermal amplification reaction was performed by maintaining the temperature at 65°C . Since no thermal cycling was involved, the fluorescence signal monotonically increased as the reaction proceeded. The Rsf-1 gene was exponentially amplified and successfully detected as shown in the real time HDA amplification curve (Fig. 8a). Again, the specificity of the amplicon was evaluated by the melting curve analysis and a single peak was observed (Fig. 8b). The HDA product was also further verified by agarose gel electrophoresis (ESI[†] Fig. S4).

Pathogen detection

As proof of principle for pathogen detection, *E. coli* was chosen as our model microorganism for testing. Pathogen detection started with gDNA extraction followed by real time PCR using a previously validated set of primers and TaqMan probe specific for the 16S rRNA gene of *E. coli*.^{49,50} The process of gDNA extraction from *E. coli* was similar to that used for extraction from blood. Because some prokaryotic cells possessed cell walls and were more resistant to lysing reagents, the lysis step was performed at 70 °C. Fluorescence of the TaqMan probe was initially quenched and was restored only when the probe was cleaved by the polymerase during the elongation. Thus, increase in fluorescence intensity suggested successful amplification of the microbial sequences. As shown in Fig. 9, the real time PCR amplification curve demonstrates successful detection of *E. coli*. The PCR amplicon was collected and further verified by agarose gel electrophoresis (ESI[†] Fig. S5). Assays to detect other clinically relevant pathogens, such as methicillin-resistant *Staphylococcus aureus* (MRSA) and *Chlamydia trachomatis* are currently underway. These pathogens are typically found in high abundance and require very minimal sample volumes.

Conclusions

In conclusion, we have demonstrated a droplet microfluidic platform that integrates sample preparation from crude biomaterials, nucleic acid amplification reaction and fluorescence based detection. The platform employs SSP both as a biomaterial carrier and droplet actuator. We have successfully detected the cancer biomarker Rsf-1 and identified pathogens from crude biosamples using real time PCR and real time HDA. The specificity was verified by melting curve analysis or using sequence specific TaqMan probe. The platform is one of the first droplet based, miniaturized and fully functional systems that have demonstrated the entire detection process from crude biosamples to results with real time readout and melting curve analysis, which we believe could be of great interest and benefit to healthcare personals. To our best knowledge, we also believe we are the first to demonstrate the real time isothermal amplification using HDA on droplet microfluidic platform. The proposed platform has several advantages. First, the surface topography assisted droplet manipulation offers a higher degree of flexibility, hence relatively large amounts of SSP can be used for efficient gDNA extraction and droplet actuation without complicating SSP splitting. Second, discrete droplets function as virtual reaction chambers and allow material transfer between droplets with the SSP acting as carriers. This material transfer scheme significantly reduces the complexity of the microfluidic devices, offers a much simpler solution to microfluidic control, and allows a higher degree of integration between multiple sample processing and reactions units. Third, the entire assay is performed from the crude biomaterials to results on a single handheld platform. The valveless and pumpless microfluidic control scheme eliminates many peripheral accessories, making the platform easily accessible at the point of care. Last, the amplification reaction is performed in an open-chamber system, which bypasses the microbubble containment modules that complicate many microfluidic PCR systems and greatly simplifies the chip design.³⁰

Acknowledgments

The authors would like to thank fundings from NIH (R21-CA120742, U54-AI057168-07 and U54CA151838), NSF (0546012, 0725528, 0730503), DARPA Micro/Nano Fluidics Fundamentals Focus (MF3) Centre, and The Hartwell Foundation.

References

1. WHO. The world health report 2004-changing history. 2004
2. Nevins JR, Huang ES, Dressman H, Pittman J, Huang AT, West M. Hum Mol Genet. 2003; 12:R153–R157. [PubMed: 12928487]
3. Ginsburg GS, McCarthy JJ. Trends Biotechnol. 2001; 19:491–496. [PubMed: 11711191]
4. Vilkner T, Janasek D, Manz A. Anal Chem. 2004; 76:3373–3385. [PubMed: 15193114]
5. Abgrall P, Gue AM. J Micromech Microeng. 2007; 17:R15–R49.
6. Craighead H. Nature. 2006; 442:387–393. [PubMed: 16871206]
7. Daw R, Finkelstein J. Nature. 2006; 442:367–367.
8. deMello AJ. Nature. 2006; 442:394–402. [PubMed: 16871207]
9. El-Ali J, Sorger PK, Jensen KF. Nature. 2006; 442:403–411. [PubMed: 16871208]
10. Janasek D, Franzke J, Manz A. Nature. 2006; 442:374–380. [PubMed: 16871204]
11. Psaltis D, Quake SR, Yang CH. Nature. 2006; 442:381–386. [PubMed: 16871205]
12. Yager P, Edwards T, Fu E, Helton K, Nelson K, Tam MR, Weigl BH. Nature. 2006; 442:412–418. [PubMed: 16871209]
13. Dittrich PS, Tachikawa K, Manz A. Anal Chem. 2006; 78:3887–3907. [PubMed: 16771530]
14. Auroux PA, Iossifidis D, Reyes DR, Manz A. Anal Chem. 2002; 74:2637–2652. [PubMed: 12090654]
15. Reyes DR, Iossifidis D, Auroux PA, Manz A. Anal Chem. 2002; 74:2623–2636. [PubMed: 12090653]
16. Rane TD, Puleo CM, Liu KJ, Zhang Y, Lee AP, Wang TH. Lab Chip. 2010; 10:161–164. [PubMed: 20066242]
17. Fan SK, Hsieh TH, Lin DY. Lab Chip. 2009; 9:1236–1242. [PubMed: 19370242]
18. Teh SY, Lin R, Hung LH, Lee AP. Lab Chip. 2009; 9:3604–3604.
19. Guttenberg Z, Muller H, Habermuller H, Geisbauer A, Pipper J, Felbel J, Kielbinski M, Scriba J, Wixforth A. Lab Chip. 2005; 5:308–317. [PubMed: 15726207]
20. Hsieh TM, Zhang Y, Pipper J, Neuzil P. microTAS 2006 conference proceeding. 2006
21. Pipper J, Inoue M, Ng LFP, Neuzil P, Zhang Y, Novak L. Nat Med. 2007; 13:1259–1263. [PubMed: 17891145]
22. Pipper J, Zhang Y, Neuzil P, Hsieh TM. Angew Chem Int Ed. 2008; 47:3900–3904.
23. Lehmann U, Vandevyver C, Parashar VK, Gijs MAM. Angew Chem Int Ed. 2006; 45:3062–3067.
24. Diehl F, Li M, He YP, Kinzler KW, Vogelstein B, Dressman D. Nat Methods. 2006; 3:551–559. [PubMed: 16791214]
25. Margulies M, Egholm M, Altman WE, Attiya S, Bader JS, Bemben LA, Berka J, Braverman MS, Chen YJ, Chen ZT, Dewell SB, Du L, Fierro JM, Gomes XV, Godwin BC, He W, Helgesen S, Ho CH, Irzyk GP, Jando SC, Alenquer MLI, Jarvie TP, Jirage KB, Kim JB, Knight JR, Lanza JR, Leamon JH, Lefkowitz SM, Lei M, Li J, Lohman KL, Lu H, Makhijani VB, McDade KE, McKenna MP, Myers EW, Nickerson E, Nobile JR, Plant R, Puc BP, Ronan MT, Roth GT, Sarkis GJ, Simons JF, Simpson JW, Srinivasan M, Tartaro KR, Tomasz A, Vogt KA, Volkmer GA, Wang SH, Wang Y, Weiner MP, Yu PG, Begley RF, Rothberg JM. Nature. 2005; 437:376–380. [PubMed: 16056220]
26. Zhang JH, Cheng ZJ, Zheng YM, Jiang L. Appl Phys Lett. 2009; 94:144104.
27. Shastry A, Case MJ, Bohringer KF. MEMS 2005 Miami: Technical Digest. 2005:694–697.
28. Velev OD, Prevo BG, Bhatt KH. Nature. 2003; 426:515–516. [PubMed: 14654830]

29. Ohashi T, Kuyama H, Hanafusa N, Togawa Y. *Biomed Microdevices*. 2007; 9:695–702. [PubMed: 17505884]
30. Zhang Y, Bailey V, Puleo CM, Easwaran H, Griffiths E, Herman JG, Baylin SB, Wang TH. *Lab Chip*. 2009; 9:1059–1064. [PubMed: 19350087]
31. Fair RB. *Microfluid Nanofluid*. 2007; 3:245–281.
32. Long Z, Shetty AM, Solomon MJ, Larson RG. *Lab Chip*. 2009; 9:1567–1575. [PubMed: 19458864]
33. Heid CA, Stevens J, Livak KJ, Williams PM. *Genome Res*. 1996; 6:986–994. [PubMed: 8908518]
34. Fedurco M, Romieu A, Williams S, Lawrence I, Turcatti G. *Nucleic Acids Res*. 2006;34.
35. Shendure J, Ji HL. *Nat Biotechnol*. 2008; 26:1135–1145. [PubMed: 18846087]
36. Zhang CS, Xu JL, Ma WL, Zheng WL. *Biotechnol Adv*. 2006; 24:243–284. [PubMed: 16326063]
37. Jeong YJ, Park K, Kim DE. *Cell Mol Life Sci*. 2009; 66:3325–3336. [PubMed: 19629390]
38. Gill P, Ghaemi A. Nucleosides, Nucleotides *Nucleic Acids*. 2008; 27:224–243. [PubMed: 18260008]
39. Vincent M, Xu Y, Kong HM. *EMBO Rep*. 2004; 5:795–800. [PubMed: 15247927]
40. Cady NC, Stelick S, Batt CA. *Biosens Bioelectron*. 2003; 19:59–66. [PubMed: 14558999]
41. West J, Boerlin M, Jadhav AD, Clancy E. *Sens Actuators, B*. 2007; 126:664–671.
42. Gijs MAM. *Microfluid Nanofluid*. 2004; 1:22–40.
43. Breadmore MC, Wolfe KA, Arcibal IG, Leung WK, Dickson D, Giordano BC, Power ME, Ferrance JP, Feldman SH, Norris PM, Landers JP. *Anal Chem*. 2003; 75:1880–1886. [PubMed: 12713046]
44. Zhang Y, Wang TH. *IEEE MEMS 2010 conference proceeding*. 2010
45. Shikida M, Takayanagi K, Honda H, Ito H, Sato K. *J Micromech Microeng*. 2006; 16:1875–1883.
46. Shih LM, Sheu JJC, Santillan A, Nakayama K, Yen MJ, Bristow RE, Vang R, Parmigiani G, Kurman KE, Trope CG, Davidson B, Wang TL. *Clin Cancer Res*. 2005; 11:9161S–9161S.
47. Zhang Y, Park S, Yang S, Wang TH. *Biomed Microdevices*. 2010; 12:1043–1049. [PubMed: 20632111]
48. Qiagen I. *BioSprint 15 DNA Handbook*. 2010 retrived online Jul 2010.
49. Yang S, Ramachandran P, Hardick A, Hsieh YH, Quianzon C, Kuroki M, Hardick J, Kecojevic A, Abeygunawardena A, Zenilman J, Melendez J, Doshi V, Gaydos C, Rothman RE. *J Clin Microbiol*. 2008; 46:1386–1390. [PubMed: 18305128]
50. Yang S, Lin S, Kelen GD, Quinn TC, Dick JD, Gaydos CA, Rothman RE. *J Clin Microbiol*. 2002; 40:3449–3454. [PubMed: 12202592]

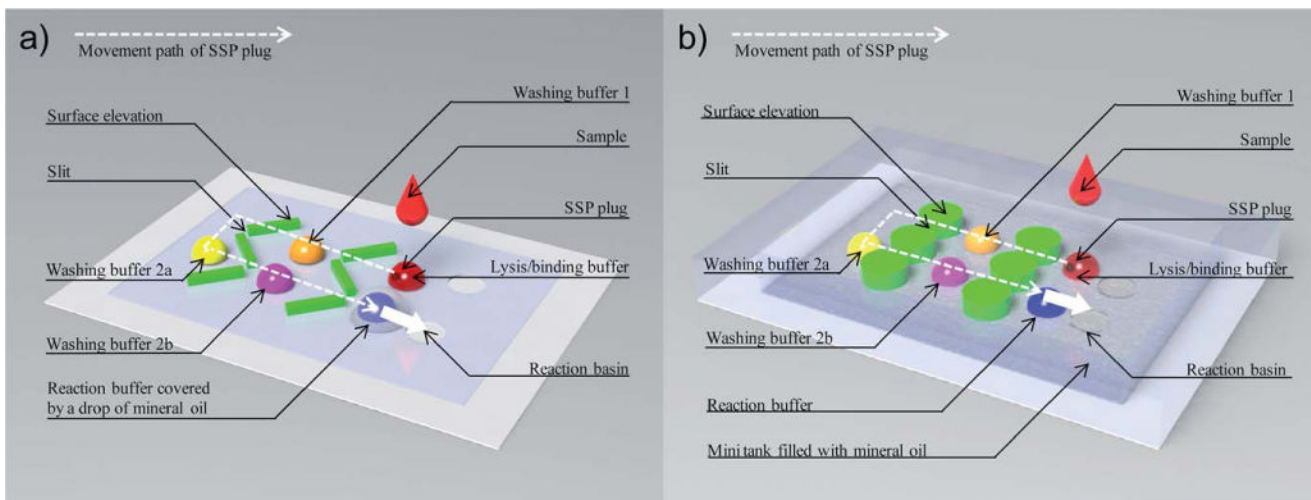


Fig. 1. Schematic illustration of microfluidic chips primed with buffer droplets for cell lysis, DNA extraction, purification and amplification. All buffer droplets were dispensed at the designated positions. (a) A device design that used V-shape slits to assist SSP splitting. All droplets sat in air except the reaction buffer droplet which was covered by mineral oil. (b) A device design that employed pairs of micro pillars to facilitate SSP splitting. The mini tank was filled with mineral oil, and all droplets sat in the oil medium. For sample preparation, the SSP moved from the lysis/binding buffer droplet to washing buffer 1, washing buffer 2a, washing buffer 2b, and ended at the amplification reaction buffer droplet. Finally, the SSP dragged the reaction buffer droplet to the micro reaction basin where the amplification reaction took place.

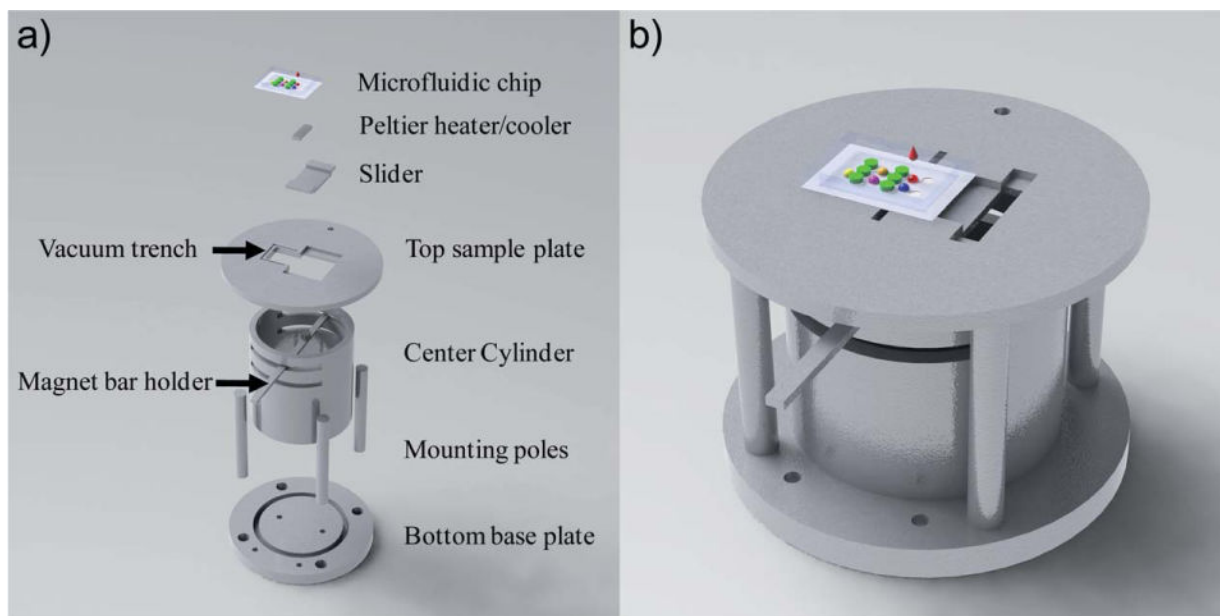


Fig. 2. CAD drawing of the sample handling stage. (a) The exploded view of the sample handling stage. (b) Assembled sample handling stage with the droplet microfluidic chip sitting on top of the Peltier heater/cooler. Photographs of the actual device are shown in the ESI[†] (Fig. S6).

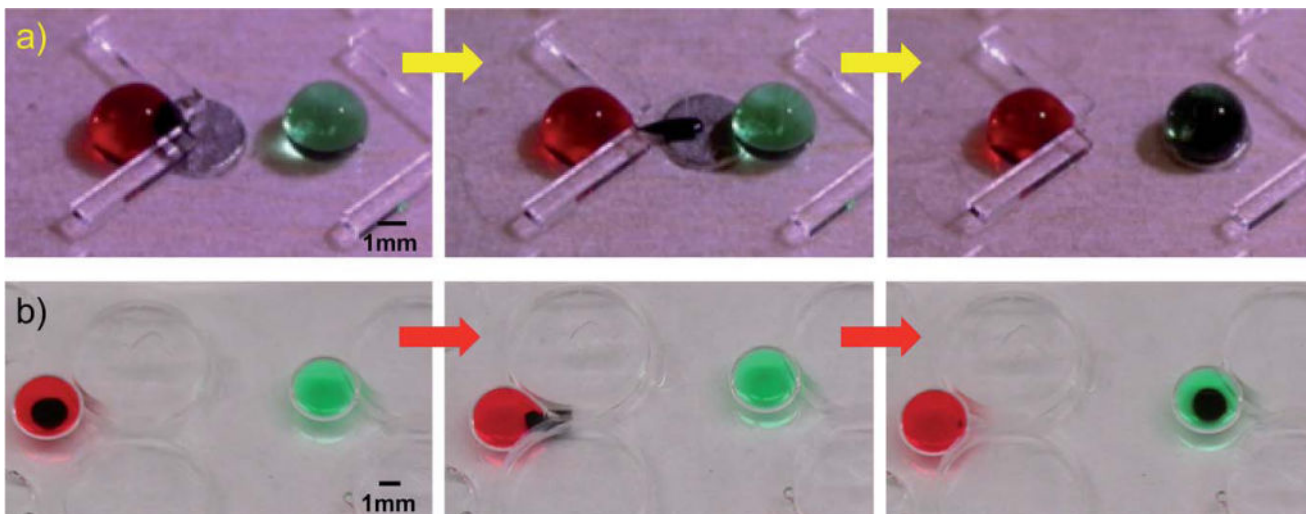


Fig. 3. Demonstration of surface topography assisted droplet manipulation. From left to right, the SSP first is mixed with the red droplet. The permanent magnet actuates the SSP which in turn drags the droplet along to the slit. The droplet is blocked by microelevations but the SSP can squeeze through the slit. After splitting from the red droplet, the SSP plug moves towards and merges with the green droplet. Two series of pictures demonstrate the surface topography assisted droplet manipulation (a) in the air medium and (b) in the oil medium respectively.

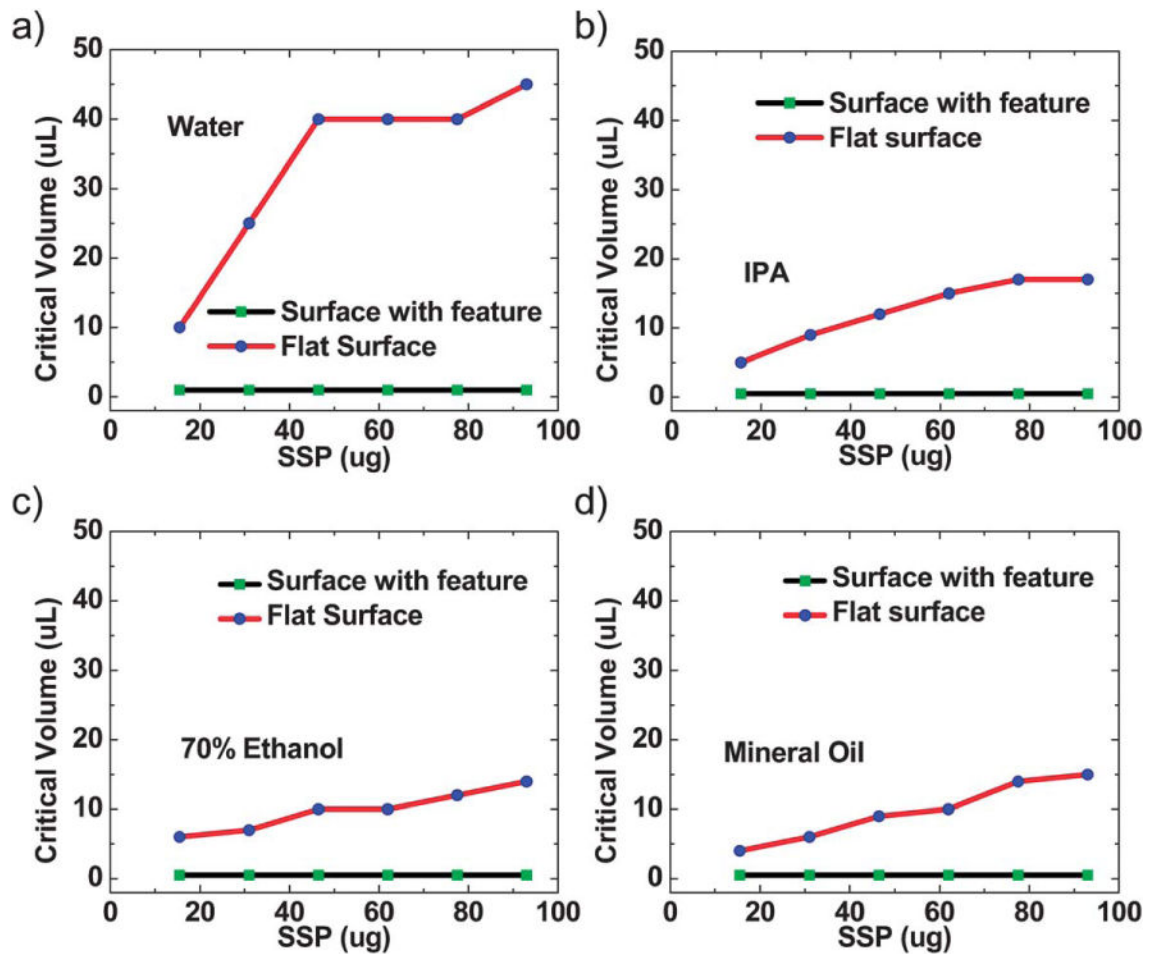


Fig. 4. Comparison of critical volumes on a flat surface and on a surface with topographic features for (a) water, (b) 100% isopropanol (IPA), (c) 70% ethanol and (d) mineral oil (Sigma Aldrich M5904) for different SSP amounts. The critical volume is defined as the smallest droplet volume below which SSP plug drags the droplet along rather than splits from the droplet.

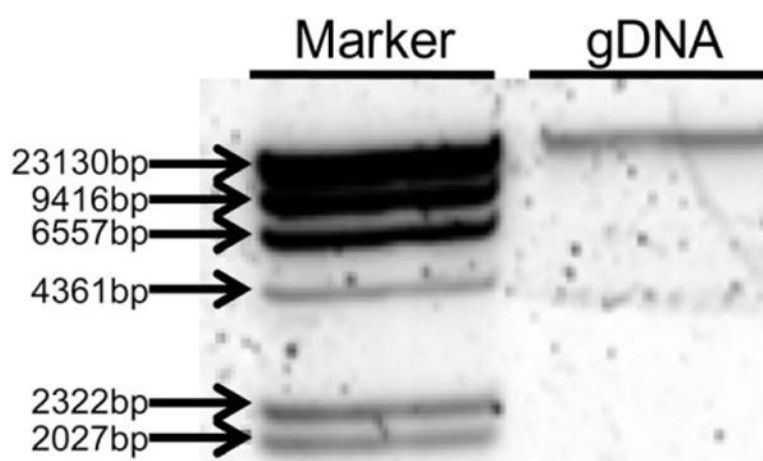


Fig. 5. The gDNA extraction was validated in a separate experiment where the extracted gDNA was collected and run on a 0.8% agarose gel with the HindIII digested IDNA as marker at 8 V cm^{-1} for 90 min.

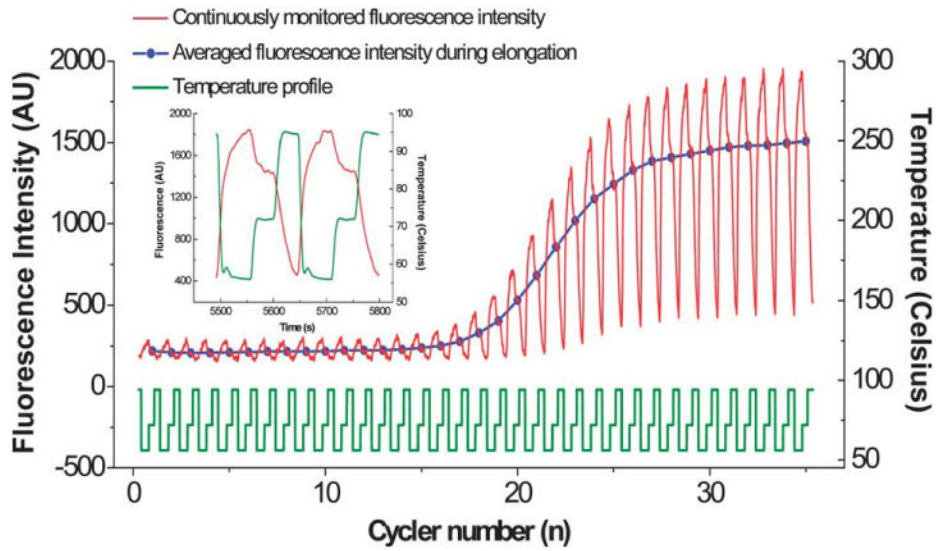


Fig. 6. Representative fluorescence and temperature profiles during thermal cycling. The fluorescence was continuously monitored at 1 Hz with 100 ms bin time. Signals at each elongation step were averaged and plotted against the thermal cycle number to obtain the real time amplification curve. The inset depicts the inverse correlation between fluorescence intensity and the temperature.

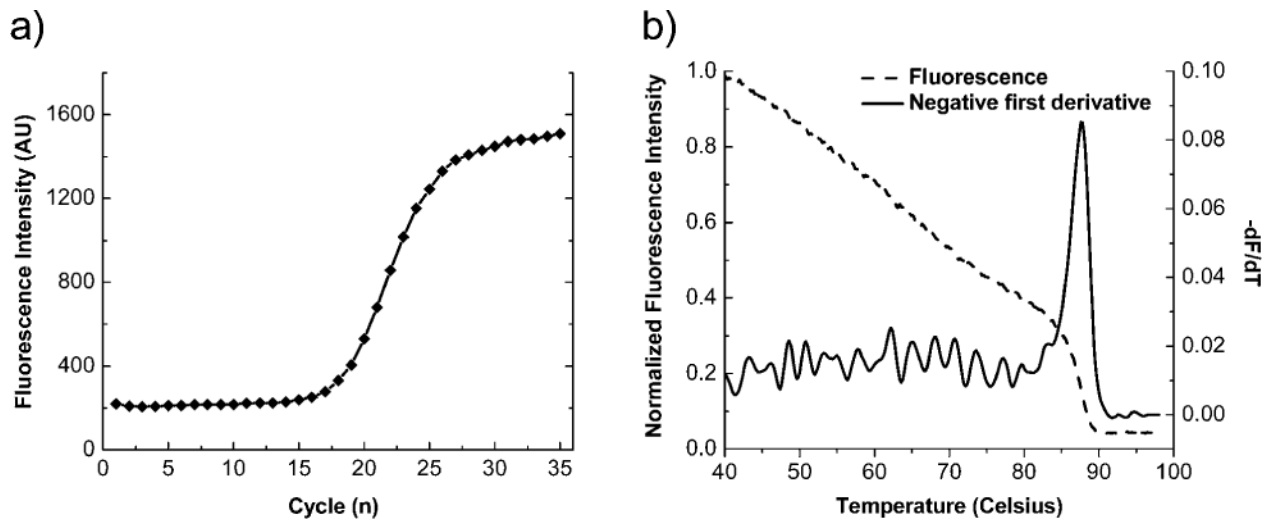


Fig. 7. Rsf-1 biomarker detection using real time PCR. (a) Real time PCR amplification curve. (b) Melting curve analysis of the amplicon.

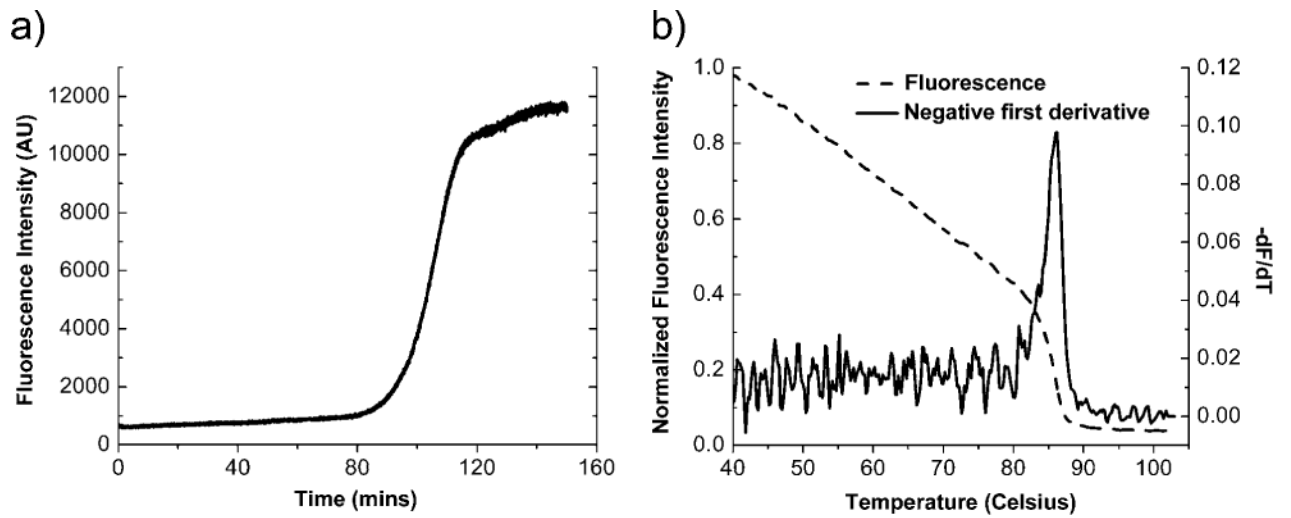


Fig. 8. Rsf-1 biomarker detection using real time HDA. (a) Real time HDA amplification curve. (b) Melting curve analysis of the amplicon.

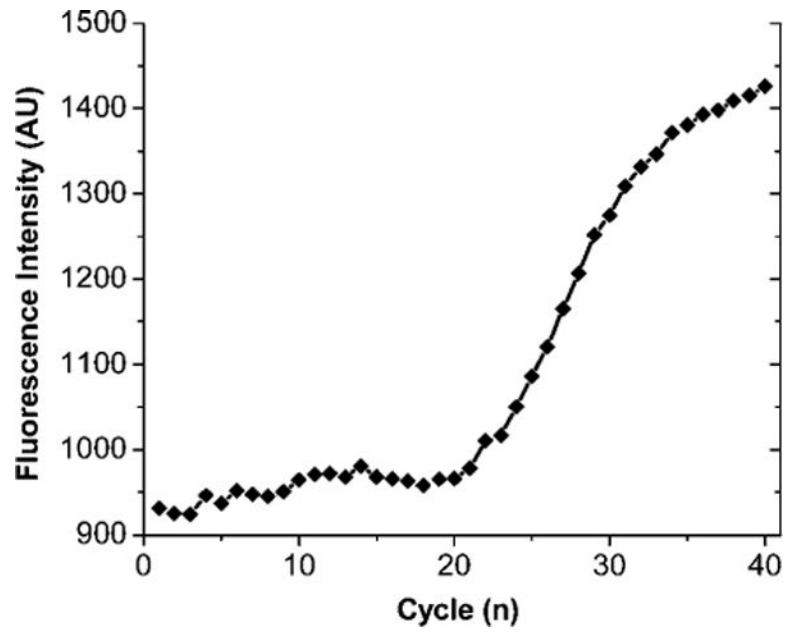


Fig. 9.
E. coli identification using real time PCR via a TaqMan probe that targets the 16s rRNA gene of *E. coli*.

Table 1

Oligonucleotide sequences

Oligonucleotide name	Sequence
PCR Rsf-1 forward primer	5'-AGTTGTGACAATGCTC ATGGAGA-3'
PCR Rsf-1 reverse primer	5'-TCTGAGGGCAG ACCCTAG-3'
HDA Rsf-1 forward primer	5'-AACCATCCCGCAA CCGCTACACC-3'
HDA Rsf-1 reverse primer	5'-AGGCTGATTGCATCTCCATGAGC-3'
<i>E. coli</i> 16S forward primer	5'-TGGAGCATGTGGTTTAATTCGA-3'
<i>E. coli</i> 16S reverse primer	5'-TGCGGGACTTAACCCAACA-3'
<i>E. coli</i> 16S Taqman primer	5'-/FAM/ACATTCTCATCTCTGAAAACCTCCGTGGATGTC/BHQ1/-3'